Transactions of the Materials Research Society of Japan 33[4] 941-944 (2008)

# A Mechanochemical Route to Synthesize $LiMn_2O_4$ as a Cathode Material for Lithium Batteries

O. Abe, Y. Hosono, T. Sano, Y. Yoshizaki
The Research Center for Superplasticity, Ibaraki University, 4-12-1 Nakanarusawa 316-8551,
Fax: +81 294 38 5078, abe@mx.ibaraki.ac.jp

Lithium manganate, $LiMn_2O_4$, applicable as a cathode material for lithium batteries has been synthesized by a redox mechanochemistry route. Gamma-$MnO_2$ shows an excellent reaction ability with LiOH under grinding and the amorphous ground product can be crystallized to $LiMn_2O_4$ at 400°C despite the requisition of the partial reduction of $MnO_2$ to $Mn^{III}Mn^{IV}O_5$. Contrary, $Mn_2O_3$ shows a poor reactivity. The dissociation of the edge-sharing chains of $MnO_6$-octahedra in γ- and β-$MnO_2$ and the increased reactivity of LiOH fused or activated under grinding is the proposed reaction mechanism. The ground products are slightly agglomerated by the moisture evolved from the hydroxide. However, the particle size can be controlled to be 300-500nm after the calcination at 800°C, when the grinding stress is limited not to be high. Unnecessarily high grinding stress induces the strong agglomeration to increase not only the size of agglomerates but the primary particle size. The synthesized $LiMn_2O_4$ with the particle size of 370nm and the crystallite of 48nm provides the good cyclic charge- discharge characteristics, while the rechargeablity of $LiMn_2O_4$ with 500nm and 68nm degrades within 3 cycles.

**Key words**: $LiMn_2O_4$, synthesis, mixing-grinding, mechanochemistry, crystallization

## 1. INTRODUCTION

Lithium manganate, $LiMn_2O_4$ is candidate as a cathode material for rechargeable lithium batteries [1,2]. This material has the peculiarity of high discharge voltage, high energy capacity, the high cost performance, and less toxicicity, but the instability of the crystalline structure of $LiMn_2O_4$ spinal under the charge-discharge cycles limits the practical application. This is due to the high sensitivity of the phase transformation to the lack of lithium ions. This instability is improved by the use of fine and well-crystalline particles.

In the present paper, the synthesis of $LiMn_2O_4$ by a mechanochemistry route has been studied, expecting the dissociation of the share-structure the $MnO_6$-octahedra or $MnO_4$-tetrahedra in the starting $MnO_2$ and $Mn_2O_3$ powders and the effect of reactive grinding aid for LiOH. The melting point of LiOH is 445°C and $MnO_2$ is reduced to $Mn_2O_3$ at 560°C. Then, if the grinding energy compatible to the thermal energy corresponding to 500°C is absorbed to the materials under grinding, we can expect the reaction products through the dissociation of the polyhedra with the reduced oxidation number of manganese ions and the reactions with the partly fused LiOH.

The reactivity of three combinations of the starting materials, γ-$MnO_2$-LiOH, γ-$MnO_2$-$Li_2CO_3$, and $Mn_2O_3$-LiOH systems, has first been tested. The influence of the grinding conditions is examined for the γ-$MnO_2$-LiOH system in some detail. The rechargeable properties are evaluated for the typical two synthesized powders with different particle size.

## 2. EXPERIMENTAL

An electrochemical $MnO_2$ (γ-$MnO_2$, Wako Pure Chem., dried at 70°C for 16h under vacuum), a reagent-grade LiOH (Merck) and $LiCO_3$ (Kanto-kagaku) were used as the starting materials. $Mn_2O_3$ was prepared by the heat-treatment of the γ-$MnO_2$ at 600°C for 3h in air. These powders were weighed (10.0g as $LiMn_2O_4$) and encapsulate -ed into the grinding vessel (stainless-steel, capacity: 420cm$^3$) with the grinding media (ϕ1, 3, 4mm YTZ balls) in a glove box filled with a dry Ar gas. Mechanochemical treatment was conduct-ed by the use of a planetary mill (Kurimoto-Tekko-Sho) with the revolution frequency ($f_{rev}$) of 3 to 6s$^{-1}$ and the fractional ball filling of 0.40. Grinding was performed for 3 to 9h with 15min cooling intervals in every 1h to keep the tempera-ture below 50°C. The detail of the planetary mill was described in the previous papers [3,4]. After the treatment, the ground products were sieved with a 100mesh Nylon screen, and dried at 85°C for 16h under vacuum. The ground products were calcined at 300-700 and 1000°C for 5h in air.

Crystalline phases of the ground products and calcined powders were identified by X-ray diffractometry (XRD, Cu$K\alpha_1$, 40kV, 20mA) and XPS (Mg$K\alpha$, 8kV, 30mA). Morphology was observed by scanning electron microscopy (SEM, Hitachi, S4300). Dehydration behavior of the ground products was examined by TG-DTA (10 K·min$^{-1}$). The specific surface area (*SSA*) was determined by a $N_2$-adsorption BET method. The electrochemical properties were measured by a potentiometer (Hokuto-denko, HA-201) at 3.5-4.3

V in Li / 1mol·dm$^{-3}$ $LiPF_6$, Ethylene carbonate+ Dimethyl carbonate(1:2) / $LiMn_2O_4$ (80mass%), Acetylene black (10mass%), Polyvinylidene fluoride cells.

## 3. RESULTS AND DISCUSSION

### 3.1 Reduction of $MnO_2$ under grinding

**Figure 1** shows the TG-DTA curves of the starting γ-$MnO_2$. Gamma-$MnO_2$ was transformed to β-$MnO_2$ showing a certain dehydration at 200-300°C, reduced to $Mn_2O_3$ at 560°C, and then $Mn_2O_3$ at 960°C in air. The mass loss at 400-800 °C was 8.7$_5$%, which agreed with the calculation (8.9$_7$%). The XRD analysis in **Fig. 2** also showed the transformation to β-$MnO_2$ at 400°C and the reduction to $Mn_2O_3$ at 600°C. The transformation also progressed under grinding. The XRD profile of ground γ-$MnO_2$ ($f_{rev}$ = 5s$^{-1}$, 3h) in Fig. 2 indicated the formation of β-$MnO_2$ with poor crystallinity. This means the dissociation of the corner-sharing double chains of $MnO_6$-octahedra in γ-$MnO_2$ to the single chains in b-$MnO_2$. The dissociation of the double chains should provide the reactive sites with LiOH, which melts at the low temperature of 445°C, under the mixing-grinding procedure. This kind of activation is not expected for $Mn_2O_3$. The reactivity of $Li_2CO_3$ with the higher melting point (618°C, accompanying with decomposition) is estimated to be less.

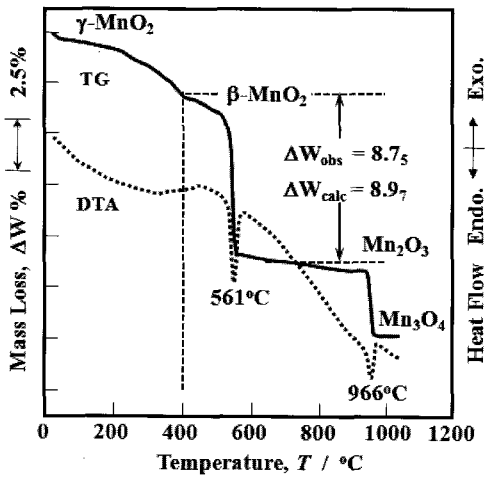


Fig.1 TG-DTA curves of the starting γ-$MnO_2$.

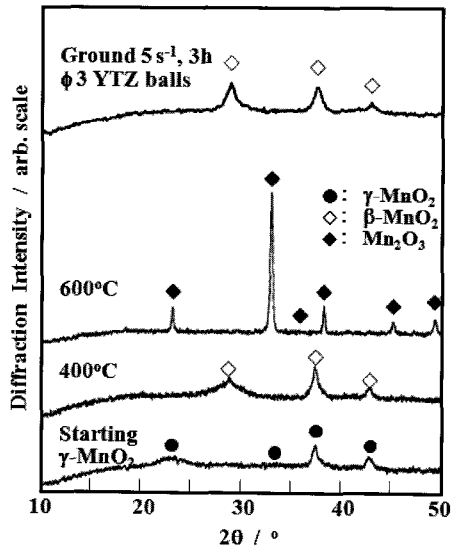


Fig.2 XRD profiles of heat-treated and ground $MnO_2$.

### 3.2 Combination of the starting materials

The XRD profiles of the ground products in γ-$MnO_2$-LiOH (GL), γ-$MnO_2$-$Li_2CO_3$ (GC) and $Mn_2O_3$-LiOH (ML) systems are sited in **Fig. 3**. The ground product GL was almost amorphous, but the increase in background was observed at 2θ = 18 and 44° in addition to the weak reflections at 2θ = 37 and 42° for β/γ-$MnO_2$. The increase in background was appeared at the diffraction angles for (111) and (400) reflections of $LiMn_2O_4$ (**Fig. 4**). The reflections for $Li_2CO_3$ were not observed for the profiles of ground product GC. ML contained the evident reflections for $Mn_2O_3$. The contamination increased as GC < GL < ML.

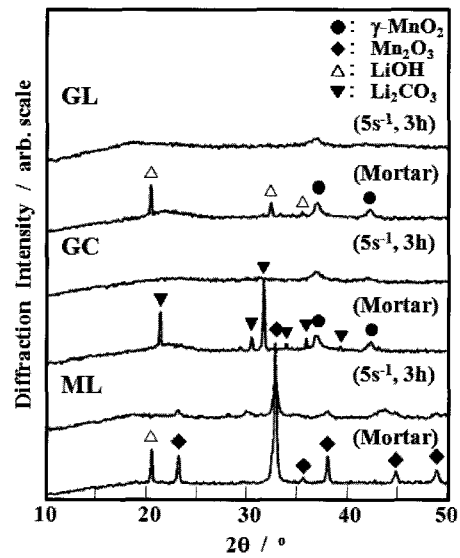


Fig.3 XRD profiles for GL, GC and ML.

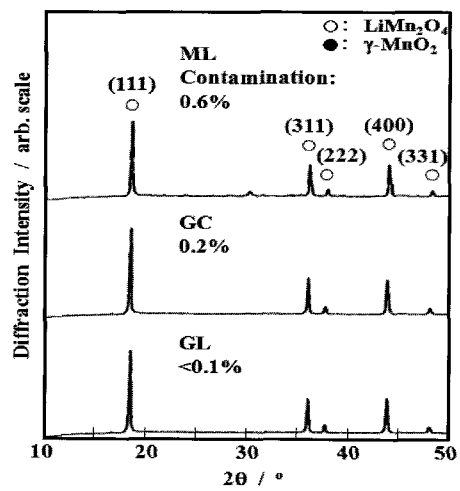


Fig.4 XRD profiles of calcined GL, GC and ML.

**Figure 5** compares the TG-DTA curves of the planetary-milled products (PM) to those of mortar ground ones (MG) in the glove box. The mortar-ground mixtures showed the typical profiles of the starting mixtures; the melting of LiOH at 450°C and the reduction of $MnO_2$ at 560°C. The drastic mass loss at 950°C was the decomposition of $LiMn_2O_4$. The planetary-milled products GL did not indicated the both changes. GC showed the slight mass loss at 560°C suggesting the less reactivity than GL. The gradual mass loss up to 400°C was due to the hydration of the ground products absorbing the moisture evolved from LiOH. The planetary-milled ML indicated the slight mass gain at 450°C. This means the reaction of $Mn_2O_3$ with fused LiOH, and $O_2$ in the ambient air. The mass loss for the dehydration of LiOH was compensated to the mass gain for oxidation of $Mn_2O_3$ to $Mn^{III}Mn^{IV}O_5$. From the above mentioned discussion, the mechanochemical reactivity is estimated in the order of GL > GC > ML.

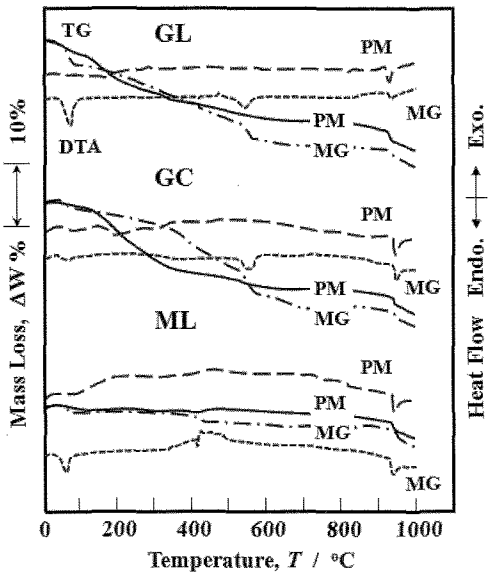


Fig.5 TG-DTA curves for GL, GC and ML.

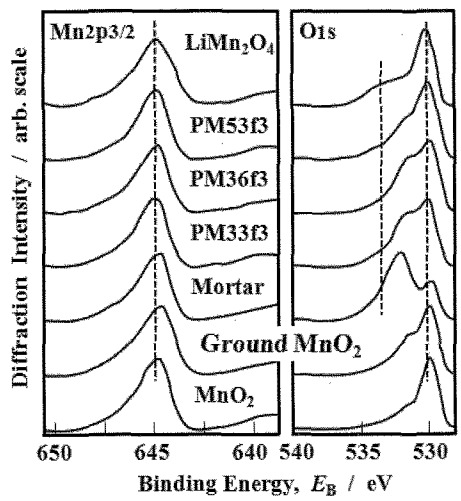


Fig.6 XPS spectra for planetary-milled products.

### 3.3 *Influence of grinding conditions*

**Figure 6** shows the $Mn2p_{3/2}$ and O1s spectra of the ground product PM33f3 ($3s^{-1}$, 3h, ϕ3mm YTZ balls as the grinding media), PM36f3 and PM53f3. The Mn2p spectra were almost identical for all samples. The peak identified to LiOH in O1s spectrum of the mortar-ground mixture disappeared for the ground products. While, the weak peak appeared at the binding energy, $E_B$ = 533eV, similar to the spectrum for $LiMn_2O_4$, meaning the formation of Li-O-Mn bond. The shoulder at $E_B$ = 532eV indicated the hydrated Mn-O bond. This shoulder became weak with the increase in grinding time (PM36f3) and the grinding stress (PM 53f3). The XRD profiles for PM33f3 in **Fig. 7** showed the direct crystallization of the ground product to $LiMn_2O_4$ without forming byproducts. Then, it was considered that hydrated $LiMn_2O_4$ formed under grinding.

The morphology of the ground products are sited in **Fig. 8**. The ground products were agglome-

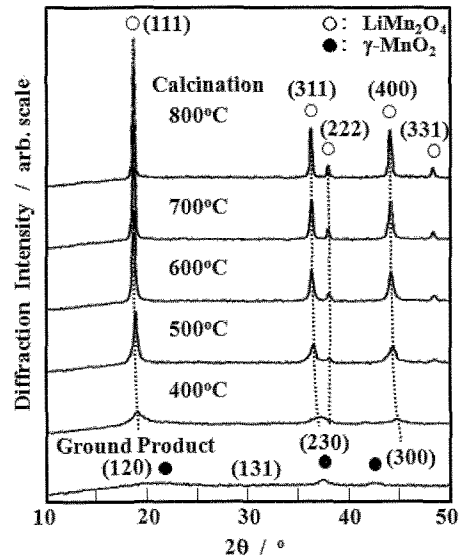


Fig.7 Crystallization of ground product PM33f3.

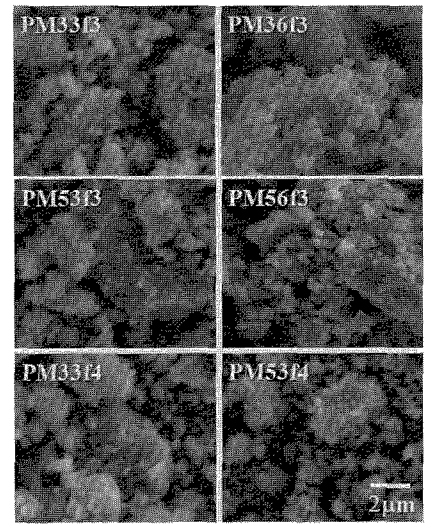


Fig.8 Morphology of calcined products (800°C).

**Table 1. Influence of grinding conditions on properties of ground and calcined products**

| | Ground product | | Calcined powder | |
|---|---|---|---|---|
| | *SSA*/m²·g⁻¹ | Δ*W*/% | *SSA*/m²·g⁻¹ | $d_{eq}$/nm |
| **Mortar mixing** | 35.6 | 18.7 | 2.8 | 510 |
| **PM33f3** | 29.2 | 13.7 | 3.7 | 380 |
| **PM36f3** | 16.4 | 13.9 | 2.1 | 670 |
| **PM53f3** | 27.9 | 15.2 | 2.8 | 500 |
| **PM56f3** | 23.7 | 10.3 | 2.5 | 560 |
| **PM59f3** | 16.7 | — | 2.2 | 640 |
| **PM33f3** | 19.9 | 13.4 | 3.1 | 450 |
| **PM53f4** | 21.4 | 12.0 | 2.9 | 480 |

***SSA*: Specific surface area, $d_{eq}$: Equivalent particle size, Δ*W*: Mass loss at 100-800°C**

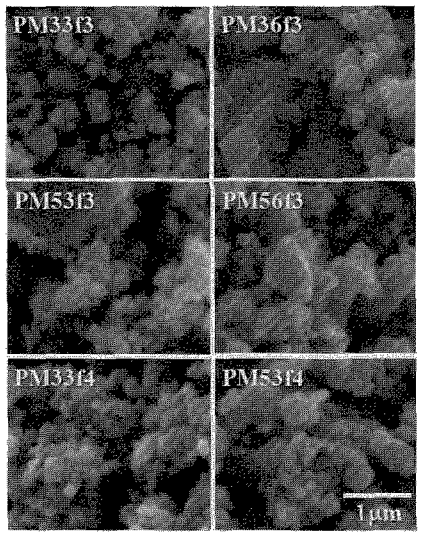


Fig.9 Morphology of ground products.

merated by the moisture evolved from LiOH. The size of the agglomerates increased with the increase in the grinding time and the revolution frequency, and decreased with the use of larger grinding media. The progress in the mechanochemical reaction forming $LiMn_2O_4$ generates the larger amount of moisture to promote the agglomeration. The *SSA* in **Table 1** decreased in the order of progressed agglomeration. The agglomerated structure succeeded to the calcined powders presented in **Fig. 9**. Although a certain agglomeration is required in the solid-state reaction mechanism proposed here, the control of the grinding atmosphere is needed to prepare fine powders. The calcined PM33f3 was well-established prismatic powder with the particle size less than 500nm (370nm in average).

### 3.4 Influence of grinding conditions

Rechargeability of the typical two synthesized $LiMn_2O_4$ powders were demonstrated in **Fig. 10** (PM33f3) and **Fig. 11** (PM53f3). PM33f3 consisted of the isolated particles having the *SSA*-equivalent particle size ($d_{eq}$) of 370nm and the crystallite size ($D$) of 48nm. PM53f3, which was synthesized with the higher grinding stress, was a little agglomerated, and the $d_{eq}$ and $D$ were 500nm and 68nm, respectively. PM33f3 showed the good rechargeability despite the two-step charge-discharge profiles. Contrary, the rechargeability of PM53f3 was markedly degraded. The mechanochemical route proposed in the present paper can be applied to the synthesis of $LiMn_2O_4$ with fine particle size and good rechargeability.

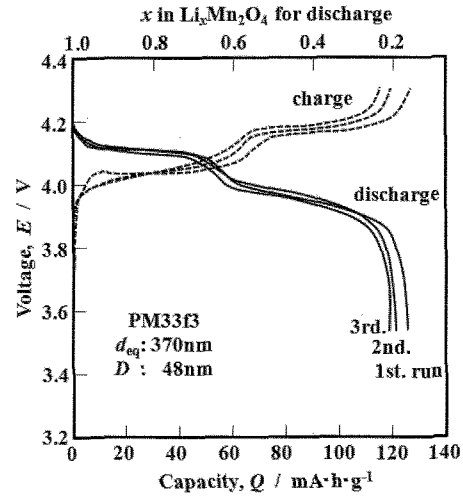


Fig.10 Rechargeability of calcined PM33f3. $d_{eq}$: equivalent particle size, $D$: crystallite size

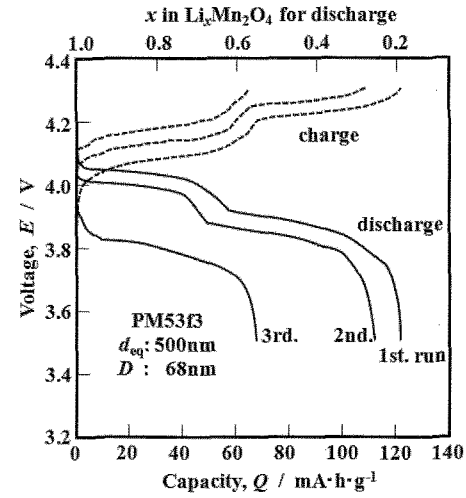


Fig.11 Rechargeability of calcined PM53f3. $d_{eq}$: equivalent particle size, $D$: crystallite size

## 4. CONCLUSION

A mechanochemical process with the peculiarity of mechanical dissociation of $MnO_6$-double chains in γ-$MnO_2$ structure and the activation of LiOH can be applied to the direct synthesis of $LiMn_2O_4$. The ground products are crystallized above 500°C. Good charge-discharge performance has been obtained for the crystallized fine powder.

### References

[1] A. Van der Ven, *et. al.*, *Solid State Ionics*, **135**, 21 (2000).
[2] T. Ohzuku, *et. al.*, *J. Electrochem. Soc.*, **137**, 769 (1990).
[3] O. Abe, *et. al*, *Trans. Mater. Res. Soc. Jpn*, **25**, 131 (2000).
[4] O. Abe, *et. al.*, *Trans. Mater. Res. Soc. Jpn*, **32**, 123 (2007).

(Recieved :January 15, 2008; Accepted June 20, 2008 )